Rotational surf zone modeling for $O(\mu^4)$ Boussinesq–Green–Naghdi systems

Yao Zhang [a], Andrew B. Kennedy [a,*], Aaron S. Donahue [a], Joannes J. Westerink [a], Nishant Panda [b], Clint Dawson [b]

[a] *Department of Civil & Environmental Engineering & Earth Sciences, University of Notre Dame, Notre Dame, IN 46556, USA*
[b] *Institute for Computational Engineering and Sciences, University of Texas at Austin, Austin, TX 78712-1229, USA*

A B S T R A C T

A surf zone model is developed and tested based on the $O(\mu^4)$ Boussinesq–Green–Naghdi system of Zhang et al. (2013). Because the model is fundamentally rotational, it uses fewer ad hoc assumptions than are found in many Boussinesq breaking wave systems. Eddy viscosity is used to describe both breaking dissipation and bottom friction, with breaking viscosities derived from the turbulent kinetic energy equation coupled with an $O(\mu^4)$ rotational wave model. In contrast, bottom friction is included by imposing the frictional coefficient-derived boundary stress as an equivalent eddy viscosity. Numerical tests for one horizontal dimension show good agreement with regular and irregular wave breaking tests, and for solitary wave runup. Surface elevation decay, setup, runup, interior orbital velocities, and depth-varying undertow velocities can all be modeled reasonably. Comparison with an $O(\mu^2)$ system shows similar performance for water surface elevations in the surf zone, demonstrating that the dissipation model is the major controlling factor. However, the $O(\mu^4)$ model shows significantly improved representations of the velocity profile in the surf zone, as expected.

© 2014 Elsevier Ltd. All rights reserved.

1. Introduction

Boussinesq-scaled water wave models give a phase resolving approximation of nearshore wave dynamics with good computational efficiency and application range. Classic depth-averaged Boussinesq theory for varying depth was introduced by Peregrine (1967), but has seen strong improvements in accuracy and range of application over the past 2 decades (Madsen and Sørensen, 1992; Nwogu, 1993; Wei et al., 1995; Kennedy et al., 2001; Madsen and Schäffer, 1998; Gobbi and Kirby, 1999; Gobbi et al., 2000; Lynett and Liu, 2002). Extensions to include wave breaking and moving shorelines were introduced into previously inviscid Boussinesq models that allowed them to simulate surf zone dynamics such as wave evolution, wave setup, and large scale wave-induced currents such as rip currents, and longshore currents. These have created systems that have provided good results for a variety of studies (e.g. Schäffer and Madsen, 1993; Sørensen et al., 1998; Chen et al., 2000; Kennedy et al., 2000a,b; Lynett et al., 2002; Musumeci et al., 2005; Nwogu and Demirbilek, 2010; Bonneton et al., 2011; Kim and Lynett, 2013).

However, most Boussinesq models feature partial or full irrotationality assumptions for orbital velocities. While reasonable for nonbreaking waves, these assumptions are strongly violated under wave breaking in the surf zone. Rotational scaling has been introduced to some Boussinesq models with additional formulations for vorticity evolution (Veeramony and Svendsen, 2000; Musumeci et al., 2005; Kim and Lynett, 2013). These can give good results, but none of these approaches has been widely adopted, which is significant as surf zone simulations require the inclusion of vorticity to provide accurate reconstructions of internal velocities. For most quasi-irrotational Boussinesq models, there are two common breaking techniques. The first is the ad hoc eddy viscosity formulation originally developed by Zelt (1991), and extended by Kennedy et al. (2000a) that yields extra viscous terms in momentum equations leading to wave dissipation. Dissipative terms have in some instances also been introduced into mass equations (Cienfuegos et al., 2010; Klonaris et al., 2013). The second technique is the surface roller approach attributed to Schäffer and Madsen (1993) based on the flux version of Boussinesq equations. This approach evolved from the roller concept introduced by Svendsen (1984) and was further developed by Madsen et al. (1997). Both eddy viscosity and surface roller techniques are of comparable accuracy. A third, more recent, approach turns off dispersive terms in the

---

* Corresponding author. Tel.: +1 574 631 6686.
  E-mail address: andrew.kennedy@nd.edu (A.B. Kennedy).

vicinity of the breaking roller and allows the dissipative nature of shallow water bores to remove energy from waves while conserving momentum (Shi et al., 2012; Tissier et al., 2012; Gallerano at al., 2014). This shallow water bore approach requires shock-capturing numerical schemes to ensure stability at the bore front but is relatively simple to implement, as it has few adjustable parameters other than criteria for switching to shallow water equations. None of these breaking schemes applied to quasi-irrotational models has well-defined velocities in the vicinity of the breaker: all assume partially irrotational velocities which is known to be untrue, and shallow water shock-capturing methods have a near-discontinuity in velocities at the bore front which leads to second order velocities being poorly defined.

An alternate but related shallow water wave theory was introduced by Green and Naghdi (1976). Using a polynomial structure of the velocity profile, the mass and momentum equations were solved in a weighted residual sense with no irrotationality constraint. Rotational Green–Naghdi equations have shown excellent nonlinear properties and very fast convergence with increasing numbers of terms in the series (Shields and Webster, 1988; Zhao et al., 2014b). However, their extreme complexity has generally confined research efforts to low levels of approximation (e.g. Ertekin et al., 1986). Although irrotational characteristics and scaling have also been introduced into the Green–Naghdi theory (Kim et al., 2003), these irrotational formulations hinder their extension to the surf zone.

In contrast, Zhang et al. (2013) developed a Boussinesq–Green–Naghdi model that shows a resemblance to both Boussinesq and Green–Naghdi systems. Polynomial expansions (Shields and Webster, 1988) and Boussinesq scaling were both applied. The systems may be extended to higher order and show excellent convergence towards exact solutions for dispersion, shoaling, and orbital velocities. Most of the asymptotic rearrangement techniques used for Boussinesq models may also be employed to improve accuracy for given levels of approximation. Importantly, the partial or complete irrotationality assumption of most Boussinesq systems was removed so that rotational surf zone flows may be modeled naturally.

In this paper, we extend the rotational Boussinesq–Green–Naghdi model (Zhang et al., 2013) to the surf zone including wave breaking and moving shorelines. Due to the rotational nature of the system, fewer assumptions are needed for vorticity and viscous terms (also called dissipative/breaking terms). Viscous terms in the Navier Stokes equation represented as eddy viscosity are kept by proper scaling to reproduce the energy dissipation under the breaking wave crest, while the eddy viscosity is modeled by the depth-integrated turbulent-kinetic-energy equation. The spatially-and-temporally-varying eddy viscosity model is coupled with the wave model to model rotational flow naturally in the surf zone. Numerous breaking tests for plunging, spilling and irregular wave breaking are shown in this paper, with computed results of surface elevation decay, setup, and depth-varying velocities showing good matches to data. A thin-layer moving shoreline technique was derived based on Benque's method (1982) and the breaking solitary wave runup simulation showed good results. Numerical tests in this paper were performed with an $O(\mu^4)$ system – this is quite unusual as most breaking wave systems have used $O(\mu^2)$ equations. Additional $O(\mu^2)$ runs for comparison purposes demonstrates the effect of the additional higher order terms on the overall system accuracy.

Because the Boussinesq class of models will never be able to simulate the complex free surfaces found in, for example, plunging breakers, there is an upper limit on accuracy, particularly in the roller region and near the wave crest. The weakly nonlinear $O(\mu^4)$ system used here also has its own accuracy limitations. For these reasons the breaking model will be intermediate in accuracy

and expense between comprehensive Navier–Stokes computational fluid dynamics models (e.g. Ma et al., 2012; Higuera et al., 2013), and the much more efficient existing Boussinesq breaking models that have more parameterized representations of breaking processes. In particular, the present methods will be able to predict internal velocities in the surf zone with more accuracy than existing Boussinesq models, but with lower cost than Navier–Stokes solvers.

2. Breaking model

2.1. Boussinesq–Green–Naghdi rotational water wave system

It is convenient to put the governing equations and the boundary conditions into dimensionless form. We define the Boussinesq-shallow water scaling for non-dimensional variables as

$$
\begin{aligned}
&(x,y) = k_0(x^*, y^*), \ z = h_0^{-1} z^*, \ t = k_0 (g_0 h_0)^{\frac{1}{2}} t^*, \ h = h_0^{-1} h^*, \\
&\eta = (h_0)^{-1} \eta^* \ P = (\rho^* g_0 h_0)^{-1} P^*, \ g = g_0^{-1} g^*, \ (u,v) = (g_0 h_0)^{-1/2} (u^*, v^*), \\
&w = (k_0 h_0)^{-1} (g_0 h_0)^{-1/2} w^* \ v_t = h_0^{-1} (g_0 h_0)^{-1/2} (k_0 h_0)^{-1} v_t^* \\
&\tau_{\mathbf{xx}} = g_0^{-1} k_0^{-2} h_0^{-3} \tau_{\mathbf{xx}}^*, \ \tau_{z\mathbf{x}} = g_0^{-1} k_0^{-1} h_0^{-2} \tau_{z\mathbf{x}}^*
\end{aligned}
\tag{2.1}
$$

where the superscript $*$ indicates dimensional variables, and g^* is gravitational acceleration. Horizontal spatial coordinates are $\mathbf{x}^* \equiv (x^*, y^*)$, while the vertical coordinate (z^*) is oriented positive upward. Time t^* is scaled by typical long wave speed $(g_0 h_0)^{1/2}$ and wavenumber k_0, while depth h^* and surface elevation η^* scale with typical water depth h_0. The pressure P^* is hydrostatically scaled. Horizontal and vertical velocities (u^*, v^*, w^*) all scale with wave orbital velocities taken from shallow water theory. This scaling assumes that the wave may be strongly nonlinear, although of course the system is also valid for small amplitude waves. Eddy viscosity v_t^* is assumed to scale with depth and gravity, and turbulent stresses use eddy viscosity scaling combined with wavenumber and depth, and velocity scales.

In the present work we use a Boussinesq–Green–Naghdi rotational water wave system that assumes a polynomial expansion for the horizontal velocity,

$$
\mathbf{u} = \sum_{n=0}^{N} \mu^{\beta_n} u_n(x, y, t) f_n(q), \quad \text{where,} \quad q = \frac{z + h(x, y)}{\eta(x, y, t) + h(x, y)}. \tag{2.2}
$$

and N is the approximation order, which must be even. The dimensionless wavenumber, $\mu = k_0 h_0$, describes how far the system is from the shallow water condition. Scaling exponent β_n gives the order of each velocity component, where $\beta_n = n$ when n is even; $\beta_n = n + 1$ when n is odd – this is the typical Boussinesq scaling for the order of μ. The polynomial basis functions $f_n(q)$ have the form $f_n = \sum_{m=0}^{n} a_{nm} q^m$, with arbitrary real constants for polynomial coefficients, a_{nm}, and $a_{nn} \neq 0$. It is assumed without loss of generality that $f_0 = 1$. The sigma-like coordinate q varies between zero at the bed and one at the free surface. All horizontal velocities components $\mathbf{u}_0, \mathbf{u}_1, \ldots, \mathbf{u}_N$ are independent so that higher order velocity components are not defined by lower order components as in standard irrotational Boussinesq theories (e.g. Peregrine, 1967). Specification of both the order of approximation, $O(\mu^N)$, and the polynomial coefficients, a_{nm}, will define the specific systems once substituted into the mass and momentum equations. In particular, different choices of a_{nm} will yield different wave properties through asymptotic rearrangement which is similar to changes in properties by using different reference velocities in Nwogu (1993). All systems will converge with an increasing order of approximation, but have different properties with different choice of basis functions.

The vertical velocity, w, is then uniquely specified from integrating the continuity equation with bottom boundary condition as

$$w = \sum_{n=0}^{N} \mu^{\beta_n} [-(\nabla \cdot \mathbf{u}_n)(h+\eta)g_n + (\mathbf{u}_n \cdot \nabla(h+\eta))r_n - (\mathbf{u}_n \cdot \nabla h)f_n] \quad (2.3)$$

where g_n and r_n are integral functions of f_n, e.g. $g_n \equiv \int_0^q f_n(q')dq'$, with many other functions defined (Appendix B). All integrals have constant of integration defined such that $g_n|_{q=0} = 0$ and thus $g_n|_0^{q=1} = g_n|_{q=1}$.

To arrive at a final system of equations, the velocity expansions, and viscous/turbulent stress approximations are inserted into the mass and momentum equations and terms are kept or discarded according to the assumed order of approximation, $O(\mu^N)$. This is identical to the procedure in Zhang et al. (2013), but retaining turbulent stresses, which must be specified through a turbulence closure.

The vertically integrated mass conservation equation is

$$\frac{\partial \eta}{\partial t} + \nabla \cdot \int_{-h}^{\eta} \mathbf{u} dz = 0. \quad (2.4)$$

which, after substitution of specific f_n, gives Eqs. (A.1), (A.3) in Appendix A for $O(\mu^2)$ and $O(\mu^4)$, respectively.

The momentum equations are then integrated in a weighted residual sense using the $N+1$ basis functions from the bed to the free surface:

$$\int_{-h}^{\eta} f_m \left(\frac{\partial \mathbf{u}}{\partial t} + \mathbf{u} \cdot \nabla \mathbf{u} + w\frac{\partial \mathbf{u}}{\partial z} + \nabla P - \mu^2 \nabla \cdot \tau_{\mathbf{xx}} - \frac{\partial}{\partial z}\tau_{zx} \right) dz = 0,$$
$$m = 0, 1, \ldots, N. \quad (2.5)$$

The nonhydrostatic pressure is found by integrating the dimensionless vertical momentum equation from z to η assuming a zero gauge pressure at the free surface

$$P(z) = \mu^2 \int_z^{\eta} \frac{\partial w}{\partial t} dz + \mu^2 \int_z^{\eta} \mathbf{u} \cdot \nabla w dz + \mu^2 \int_z^{\eta} w\frac{\partial w}{\partial z} dz$$
$$- \mu^2 \int_z^{\eta} \left(\nabla \cdot \tau_{\mathbf{zx}} + \frac{\partial}{\partial z}\tau_{zz} \right) dz + g(\eta - z) \quad (2.6)$$

After substitution and integration, these give the coupled momentum Eqs. (A.2) and (A.4) in Appendix A for $O(\mu^2)$ and $O(\mu^4)$, respectively. The systems resemble coupled lower order Boussinesq equations. Unlike standard Boussinesq expansions, rotational processes are included and evolve naturally once turbulent stresses τ_{ij} are specified. This involves determination of the breaking terms and bottom friction through models for turbulent viscosity and its evolution, subject to scaling and complexity limitations.

2.2. Breaking terms and bottom friction

The breaking model developed here aims at a state intermediate between Boussinesq models with eddy viscosity breaking terms inserted after the model derivation and calibrated to give reasonable wave heights in the surf zone (Kennedy et al., 2000a; Lynett et al., 2002), and more sophisticated computational fluid dynamics models with complex turbulence closures. The goals of the present model are to provide accurate wave heights, water levels, and internal water velocities in the surf zone while retaining a reasonable computational cost and implementational complexity within the Boussinesq–Green–Naghdi framework. The system will not attempt to simulate detailed turbulence properties, or to represent the bottom boundary layer. The basic framework of the present model will use eddy viscosity with a $k - l$ turbulence model, with mixing length l a function of water depth.

Significant simplifications must be imposed to arrive at a tractable model:

- Turbulent terms in the pressure Eq. (2.6) are neglected,
- Bottom stresses and wave breaking will be treated as separate terms, with different evolution equations, and acting on different portions of the system,
- Only leading order vertical velocity terms are retained.

This division between breaking and bottom friction has a physical basis, as bottom stresses are bed-generated and diffuse upwards while wave breaking arises from surface processes and diffuses downwards (e.g. Richard and Gavrilyuk, 2012). In the wave roller, breaking stresses will dwarf the much smaller bottom-generated shear stresses, while breaking stresses are small outside the roller where the bottom stresses dominate. The neglect of turbulent stresses in the pressure equation, while making the system more tractable, also has a physical basis: turbulent (or any) pressures generate only normal stresses and thus will not contribute to the vorticity generation leading to depth-varying currents. Together, these simplifications will reduce the generality of the system and mean that details of pressures and turbulent stresses will be more simplified than reality; however, the single-valued free surface in this and many other models means that representation of plunging jets, other free surface complexities such as surface turbulence, and their effects will always have an upper limit on accuracy in the surf zone. The additional approximations will allow the ability to model important aspects of both current-related shear and roller-related dissipation in the surf zone, which are the two most important aspects desired.

Because breaking dissipation and bottom stress effects are separated, they will be modeled with separate eddy viscosities, $v_{t1}(\mathbf{x}, t)$, and $v_{t2}(\mathbf{x}, z, t)$, respectively. Applying these assumptions to the eddy viscosity approximation, and assuming that eddy viscosity scaling is $O(v_t) = O(\mu h_0(gh_0)^{1/2})$, the respective turbulent stress terms become

$$\mu^2 \nabla \cdot \tau_{\mathbf{xx}} = \mu^2 \nabla \cdot \left[v_{t1} \left(\nabla \mathbf{u} + (\nabla \mathbf{u})^T \right) \right] \quad (2.7)$$

$$\frac{\partial}{\partial z}\tau_{\mathbf{xz}} = \frac{\partial}{\partial z} \left[v_{t2} \left(\mathbf{u}_z + \mu^2 \nabla w \right) \right] \quad (2.8)$$

In order to include a specified bottom friction, the bottom stress-generated term in Eq. (2.5) is integrated by parts,

$$\int_{-h}^{\eta} f_m \frac{\partial \tau_{\mathbf{xz}}}{\partial z} dz = \int_{-h}^{\eta} \frac{\partial}{\partial z} (f_m \tau_{\mathbf{xz}}) dz - \int_{-h}^{\eta} \frac{\partial f_m}{\partial z} \tau_{\mathbf{xz}} dz$$
$$= (f_m \tau_{\mathbf{xz}})|_{-h}^{\eta} - \int_{-h}^{\eta} \frac{\partial f_m}{\partial z} v_{t2}(\mathbf{x}, z) \left(\mathbf{u}_z + \mu^2 \nabla w \right) dz. \quad (2.9)$$

If there is no air–water shear stress, then $\tau_{xz}(\eta) = 0$. For bottom frictional dissipation, some sort of information is required based on bottom conditions, whether from bed roughness or vegetation type. These are often placed into a drag framework such as $\tau_{xz}(-h) = C_f \mathbf{u}_b |\mathbf{u}_b|$, where $\mathbf{u}_b$ is the near-bottom velocity, and C_f is a bottom friction coefficient normally in the order of 10^{-3}, and this approach will be adopted. A bottom stress coefficient and gradient also imply a vertical profile for the eddy viscosity, $v_{t2}(\mathbf{x}, z) = \bar{v}_{t2}(\mathbf{x})f_v(q)$. Combining eddy viscosity and bottom friction, the depth-varying eddy viscosity will then be $v_{t2}(\mathbf{x}, z) = \epsilon f_v C_f(\eta + h)|\mathbf{u}_b|$, where ϵ is a constant applied to control the velocity difference between surface and bed, and the influence of the bed velocity (or alternatively mean velocity) on eddy viscosity arises from scaling considerations. The simplest application will be a constant vertical profile $f_v(q) = 1$ (e.g. Kim and Lynett, 2013), which will use $\epsilon \approx 0.4$, but other vertical profiles may also be employed.

Using these vertical variations for v_{t1} and v_{t2} and performing integrations over depth, the turbulent stresses retained are then

$$
\begin{aligned}
\int_{-h}^{\eta} f_m \frac{\partial \tau_{xz}}{\partial z} dz &= -f_m|_{q=0} C_f \mathbf{u}_b |\mathbf{u}_b| - \int_0^1 f_m' (v_{t2} \mathbf{u}_{,q}/(\eta+h) + \mu^2 v_{t2} \nabla w) dq \\
&= -f_m|_{q=0} C_f \mathbf{u}_b |\mathbf{u}_b| - \epsilon C_f |\mathbf{u}_b| \sum_{n=0}^{N} \mu^{\beta_n} \mathbf{u}_n \psi_{mnv}|_0^1 \\
&\quad + \mu^2 \epsilon C_f |\mathbf{u}_b| (\eta+h) \Big[\nabla(\nabla \cdot \bar{\mathbf{u}}_0)(\eta+h) \varepsilon_{vm}|_0^1 \\
&\quad + (\nabla \cdot \mathbf{u}_0 \nabla h + \nabla(\mathbf{u}_0 \cdot \nabla h)) \zeta_{vm}|_0^1 \Big]
\end{aligned}
\tag{2.10}
$$

and

$$
\begin{aligned}
\int_{-h}^{\eta} \mu^2 f_m \nabla \cdot \tau_{xx} dz &= \int_{-h}^{\eta} \mu^2 f_m \nabla \cdot \left(v_t \left(\nabla \mathbf{u} + (\nabla \mathbf{u})^T \right) \right) dz \\
&= \mu^2 \nabla \cdot \left[(\eta+h) \int_0^1 f_m v_{t1} (\nabla \mathbf{u} + (\nabla \mathbf{u})^T) dq \right] \\
&\quad - \mu^2 (\eta+h) \int_0^1 v_{t1} (\nabla f_m) \cdot (\nabla \mathbf{u} + (\nabla \mathbf{u})^T) dq \\
&\quad - \mu^2 f_m v_{t1} (\nabla \eta) \cdot (\nabla \mathbf{u} + (\nabla \mathbf{u})^T)|_{q=1} \\
&\quad - \mu^2 f_m v_{t1} (\nabla h) \cdot (\nabla \mathbf{u} + (\nabla \mathbf{u})^T)|_{q=0} \\
&= \sum_{n=0}^{N} \mu^{\beta_n+2} \nabla \cdot \Big[v_{t1} (\eta+h)(\nabla u_n + (\nabla u_n)^T) \phi_{mn}|_0^1 \\
&\quad + v_{t1}(u_n^T \nabla^T + (u_n^T \nabla^T)^T) \Big(h \zeta_{mn}|_0^1 - (\eta+h) \varepsilon_{mn}|_0^1 \Big) \Big] \\
&\quad - \sum_{n=0}^{N} \mu^{\beta_n+2} v_{t1} \Big[(\zeta_{nm}|_0^1 \nabla h - \varepsilon_{nm}|_0^1 \nabla(\eta+h)) \\
&\quad \cdot (\nabla u_n + (\nabla u_n)^T) + (E_{mn}|_0^1 \nabla h - J_{mn}|_0^1 \nabla(\eta+h)) \\
&\quad \cdot (u_n^T \nabla^T h + (u_n^T \nabla^T)^T h)/(\eta+h) - (J_{mn}|_0^1 \nabla h - K_{mn}|_0^1 \nabla(\eta+h)) \\
&\quad \cdot (u_n^T \nabla^T (\eta+h) + (u_n^T \nabla^T)^T (\eta+h))/(\eta+h) \Big] \\
&\quad + \sum_{n=0}^{N} \mu^{\beta_n+2} v_{t1} (f_m \nabla q)|_0^1 \cdot \Big[(\nabla u_n + (\nabla u_n)^T)(\eta+h) f_n|_0^1 \\
&\quad + (u_n^T \nabla^T + (u_n^T \nabla^T)^T)(h - (\eta+h) q|_0^1) f_n'|_0^1 \Big]
\end{aligned}
\tag{2.11}
$$

2.3. $k - l$ Turbulent-kinetic-energy model for v_{t1}

The final stage of the breaking model is the evolution equation for eddy viscosity, v_{t1}. This arises directly from representations for turbulent kinetic energy evolution combined with assumptions and simplifications relevant to the structure of the Boussinesq–Green–Naghdi system and eddy viscosity. The $k - l$ model is arguably the simplest incomplete turbulence model, and hence it has a broad range of applicability with a low computational cost (e.g. Pope, 2003). Similarly to $k - \epsilon$ model, $k - l$ is a favorable numerical coupling between the flow and turbulence equations with the term, $v_t \left(\frac{\partial \langle U_i \rangle}{\partial x_j} + \frac{\partial \langle U_j \rangle}{\partial x_i} \right)$. This actually allows us to get better velocity profile under breaking and comparable computational efficiency compared to most other Boussinesq-type model. The process of production, transport and dissipation equation for the turbulent kinetic energy k can be expressed as Pope (2003)

$$
\frac{Dk}{Dt} \equiv -\nabla \cdot \mathbf{T}' + \mathcal{P} - \varepsilon.
\tag{2.12}
$$

Here, the turbulent energy flux $\mathbf{T}'$ is modeled with a gradient-diffusion hypothesis as

$$
\mathbf{T}' = -\frac{v_{t1}}{\sigma_k} \nabla k.
\tag{2.13}
$$

where σ_k is the turbulent Prandtl number for kinetic energy, and is generally taken to be 1.0. According the turbulent-viscosity hypoth-

esis introduced by Boussinesq (1877), the production of turbulent kinetic energy is then

$$
\mathcal{P} = v_{t1}[\nabla \mathbf{u} \cdot (\nabla \mathbf{u} + (\nabla \mathbf{u})^T) + 2\mathbf{u}_{,z} \cdot \nabla w + \frac{1}{\mu^2} \mathbf{u}_{,z} \cdot \mathbf{u}_{,z} + 2w_{,z}^2].
\tag{2.14}
$$

where $O(\mu^2)$ terms are neglected. The turbulent viscosity is defined by Pope (2003)

$$
v_{t1} = ck^{1/2} \bar{l}_m.
\tag{2.15}
$$

where $\bar{l}_m$ is the vertically averaged mixing length, l_m. At high Reynolds number the dissipation rate is modeled as

$$
\varepsilon = C_\varepsilon k^{3/2} / \bar{l}_m.
\tag{2.16}
$$

where $C_\varepsilon = c^3$ in $k - l$ model. Nezu and Rodi (1986), based on experimental measurements made with stationary currents, concluded that the length scale tends to zero near the water surface. The increase of the mixing length and its reduction near the free surface is given by

$$
l_m = \kappa q \sqrt{1-q}(\eta+h)
\tag{2.17}
$$

$$
\bar{l}_m = \int_0^1 l_m dq = 4/15 \kappa (\eta+h)
\tag{2.18}
$$

where $\kappa = 0.412$ (von Karman constant).

After inserting expressions for T', $\mathcal{P}$, ϵ into (2.12) and substituting v_{t1} for k, the dimensionless TKE approximation equation transforms to

$$
\frac{Dv_{t1}}{Dt} = \frac{\mu}{v_{t1}\sigma_k} \nabla \cdot (v_{t1}^2 \nabla v_{t1}) + \mu \frac{c^2 \bar{l}_m^2}{2v_{t1}} \mathcal{P} - \frac{1}{\mu} \frac{c^2}{2\bar{l}_m^2} v_{t1}^2
\tag{2.19}
$$

A value of $c = 0.55$ yields the correct behavior for shear flow in $k - l$ models, and this is used here. As assumed above, kinematic viscosity is depth-uniform. Integrating (2.19) from bottom to the surface then gives

$$
\begin{aligned}
&\frac{\partial v_{t1}}{\partial t} + \nabla v_{t1} \cdot \sum_{n=0}^{N} \mathbf{u}_n g_n|_0^1 - \frac{\mu}{v_{t1}\sigma_k} \nabla \cdot (v_{t1}^2 \nabla v_{t1}) - \mu \frac{c^2 \bar{l}_m^2}{2v_{t1}} \int_0^1 \mathcal{P} dq \\
&\quad + \frac{1}{\mu} \frac{c^2}{2\bar{l}_m^2} v_{t1}^2 = 0.
\end{aligned}
\tag{2.20}
$$

where

$$
\begin{aligned}
\int_0^1 \mathcal{P} dq &= v_{t1} \Bigg\{ \sum_{n=0}^{N} \sum_{m=0}^{N} \mu^{\beta_m + \beta_n} \Big[\nabla \mathbf{u}_m \cdot (\nabla \mathbf{u}_n + (\nabla \mathbf{u}_n)^T) \phi_{mn}|_0^1 \\
&\quad + \nabla \mathbf{u}_m \cdot \left((\mathbf{u}_n + (\mathbf{u}_n)^T)(\nabla h \zeta_{mn} - (\eta+h) \varepsilon_{mn})|_0^1 \right) \\
&\quad + \mathbf{u}_m (\nabla h \zeta_{mn} - (\eta+h) \varepsilon_{mn})|_0^1 \cdot (\nabla \mathbf{u}_n + (\nabla \mathbf{u}_n)^T) \\
&\quad + \int_0^1 \mathbf{u}_m \nabla f_m \cdot (\mathbf{u}_n \nabla f_n + (\mathbf{u}_n \nabla f_n)^T) dq \Big] - \sum_{n=0}^{N} \mu^{\beta_n} 2\mathbf{u}_n \cdot [\nabla(\nabla \cdot \bar{\mathbf{u}}_0) r_n|_0^1 \\
&\quad + (\nabla \cdot \mathbf{u}_0 \nabla h + \nabla(\mathbf{u}_0 \cdot \nabla h))/(\eta+h) f_n|_0^1] + \sum_{n=0}^{N} \sum_{m=0}^{N} \mu^{\beta_m + \beta_n - 2} \mathbf{u}_m \\
&\quad \cdot \mathbf{u}_n/(\eta+h)^2 E_{mn}|_0^1 + 2 \Big((\nabla(\nabla \cdot \mathbf{u}_0)(\eta+h))^2/3(\nabla \cdot \mathbf{u}_0 \nabla h \\
&\quad + \nabla(\mathbf{u}_0 \cdot \nabla h))^2 + 2\nabla(\nabla \cdot \mathbf{u}_0)(\eta+h)(\nabla \cdot \mathbf{u}_0 \nabla h + \nabla(\mathbf{u}_0 \cdot \nabla h))) \Big\}.
\end{aligned}
\tag{2.21}
$$

This one equation model for the evolution of eddy viscosity is used to find depth-averaged values to use in the velocity calculations for the Boussinesq–Green–Naghli rotational wave model.

3. Moving shoreline

For computations of wave runup, a moving shoreline method is developed here. Benque et al. (1982) proposed a way to treat the
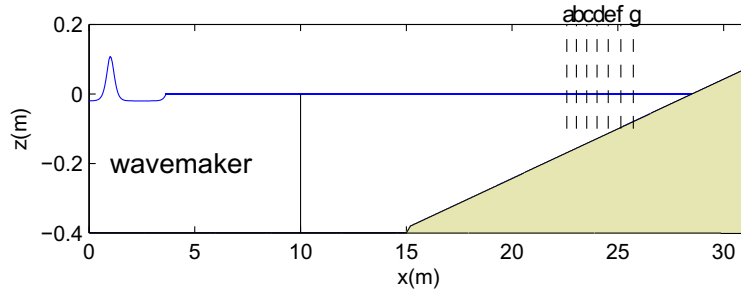
Fig. 1. Experimental setup for regular wave breaking test. Gauges (a–g) are at still water depths [0.169, 0.156, 0.142, 0.128, 0.113, 0.096, 0.079] m, respectively.

moving boundary by assuming a thin water layer over the dry land region so that all grids in the computational domain are always wet so that there is no need to update the wet computational boundary during the computation. The method we are using is similar but a bit different in the governing equations for the "thin layer". Like most moving shoreline methods, a threshold, δ, to determine the dividing point between wet and dry area needs to be set. If the total water depth $h + \eta > \delta$, the model Eqs. (2.4) and (2.5) will be applied; otherwise, a new set of equations will be adopted as following,

$$\eta = -h + \delta, \tag{3.1}$$

$$\frac{\partial u}{\partial t} = \omega(0 - u). \tag{3.2}$$

These equations set a thin layer over the "dry area" $(h + \eta <= \delta)$ allowing the water to propagate up to the shoreline but preventing the thin layer water to flow back down by setting a damping coefficient ω for the horizontal velocity, where $\omega = C(x - x(\delta))$. So unlike Benque's method, we do need to update the threshold position the at each computing time step and the total mass is better conserved.

4. Numerical verification

Here we present three numerical tests to validate the performance of the breaking model, all for one horizontal dimension.

The first test examines regular wave breaking on plane slopes as reported by Ting and Kirby (1995, 1996) for plunging and spilling cases, and compares both surface elevations and interior fluid velocities. The second test compares computed and measured irregular wave evolution over the conditions of Mase and Kirby (1992). The final test examines solitary wave runup on a beach (Synolakis, 1987).

All numerical tests used a weakly nonlinear $O(\mu^4)$ Boussinesq–Green–Naghdi rotational system (Zhang et al., 2013) with second order spatial central differencing scheme and fourth order Runge–Kutta time differencing. For all quantities in the Ting and Kirby experiments, results were also computed using a fully nonlinear $O(\mu^2)$ system to compare with the $O(\mu^4)$ data. A spatial resolution of x = 0.025 m and t = 0.02 s was used for all tests shown here.

4.1. Wave breaking

Fig. 1 shows the experimental setup where regular waves were generated in a water depth of 0.4 m using second order generation (Zhang et al., 2014a) and propagated to the 1:35 sloping beach. Two cases were studied.

1. Spilling breaker, H = 12.5 cm; T = 2 s, $kh = 0.680$,
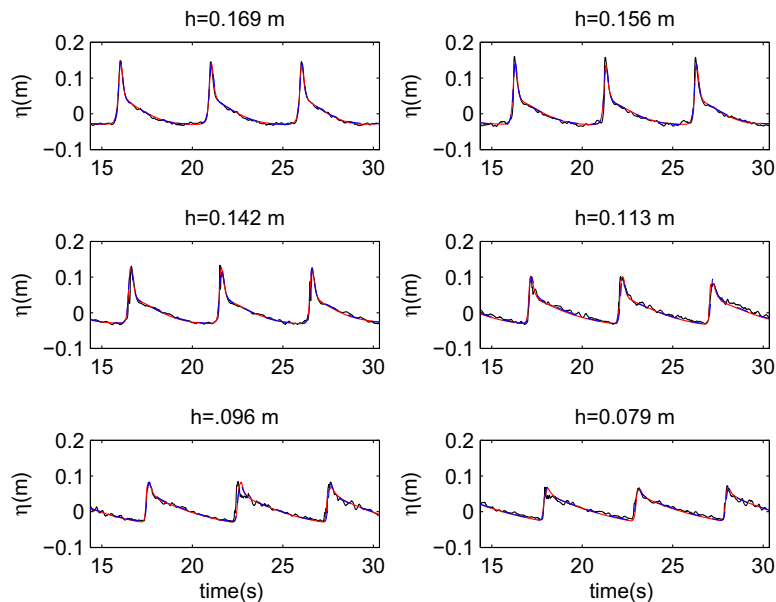2. Plunging breaker, H = 12.8 cm; T = 5 s, $kh = 0.257$.

Fig. 2. Surface elevation decay for Plunging Breaking. (—) $O(\mu^4)$; (– –) $O(\mu^2)$; (–) measured. Some lines are obscured.
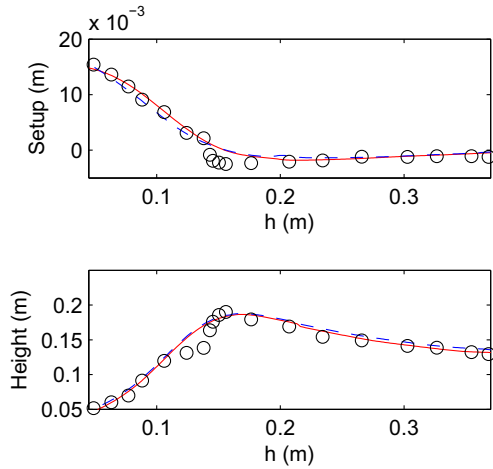
Fig. 3. Wave heights and setup for Plunging Breaking. (—) $O(\mu^4)$; (- -) $O(\mu^2)$; (o) measured.
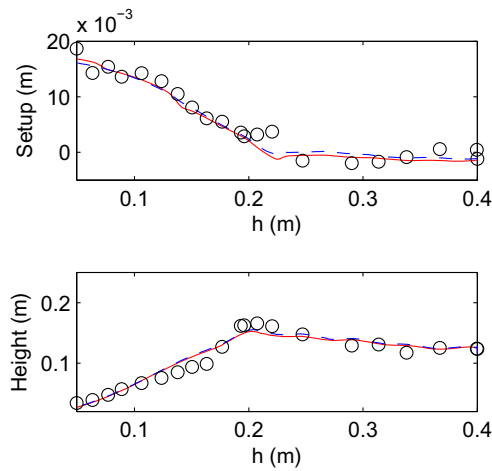

Fig. 4. Wave heights and setup for Spilling Breaking. (—) $O(\mu^4)$; (- -) $O(\mu^2)$ computed; (o) measured.

The wave height-depth ratio in the constant-depth region was large ($H/h > 0.3$) and the breaking was intense. Fig. 2 shows measured and computed time series of surface elevation at different depths for the plunging breaker case, with good agreement seen.

Figs. 3 and 4 show numerical and measured results for wave height and setup from outside the breaking region through to the shoreline, with good agreement for both quantities. Wave heights increased slowly before breaking and then rapidly decayed through the surf zone. Setup increased strongly after breaking as expected, with good agreement between computed and measured values. For both the spilling and plunging breakers, the present system does not model the very sharp decrease in wave height at initial breaking, and shows a more gradual decline. This is likely because of the time needed to build up turbulent kinetic energy using the present breaking model, which acts on velocity gradients and does not model the initial overturning. However, overall agreement is good and is comparable to other systems (Tissier et al., 2012). In somewhat of a surprise, wave heights and setups are almost identical for $O(\mu^2)$ and $O(\mu^4)$ systems. This suggests that the breaking model dominates evolution in the surf zone, and the specific equations used are of much less importance, at least for the cases considered. Because both test cases have relatively small wavenumbers even in the initial depth ($kh = 0.680$, $kh = 0.257$), both $O(\mu^2)$ and $O(\mu^4)$ systems should have similar properties for these cases, at least to second order (Zhang et al., 2013). Thus it seems that $O(\mu^4)$ systems may not always provide much of an improvement in the computation of surface elevations in the surf zone. However, as will be seen very soon, interior velocities and undertow benefit significantly from the increase from $O(\mu^2)$ to $O(\mu^4)$ systems.

One of the major benefits of Boussinesq–Green–Naghdi systems is the removal of the irrotationality assumption - thus we expect to simulate well the interior water velocities well under breaking. Here we choose two numerical results for orbital velocities: time-varying velocities at different levels, and time-averaged undertow. Fig. 5 compares the time series of horizontal velocity to the data reported by Ting and Kirby (1994) for the plunging case. The location was at water depth $h = 0.079$ m where the breaking
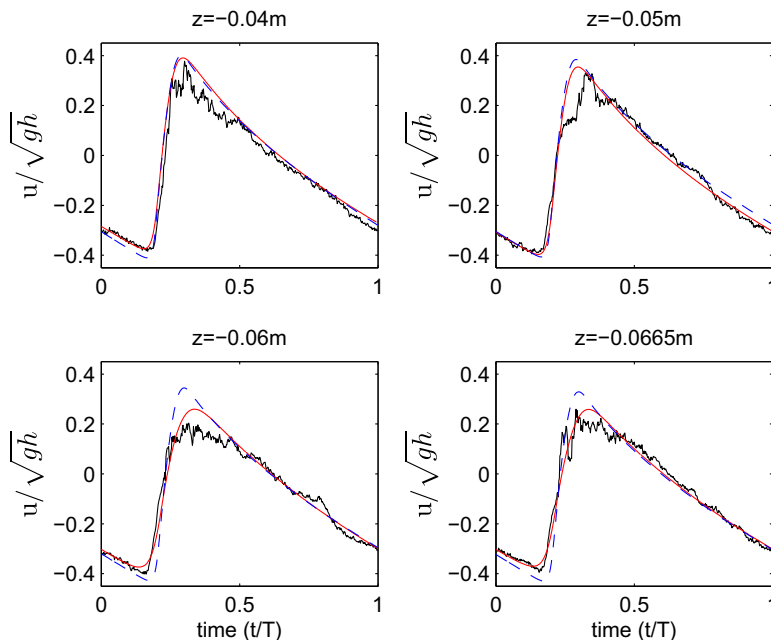

Fig. 5. Time-varying horizontal velocity for plunging breaker at different points in the water column. $h/h_b = 0.584$, $h = 0.079m$. (—) computed u_{μ^4}; (- -) computed u_{μ^2}; (–) measured.
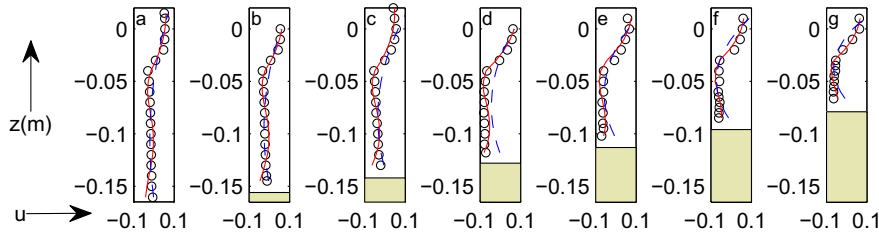
Fig. 6. Variation of dimensionless undertow velocity $\bar{u}/\sqrt{gh}$ with depth for plunging breaking. (—) $O(\mu^4)$; (- -) $O(\mu^2)$ computed; (o) measured.

Table 1
Dimensionless, depth-averaged, root-mean-square error in undertow profiles $\left(\frac{(\bar{u}_{\mu n}-\bar{u})^2}{gh}\right)^{1/2}$ for plunging breaker using $O(\mu^2)$ and $O(\mu^4)$ systems.

System	Still Water Depth						
	0.169 m	0.156 m	0.142 m	0.128 m	0.113 m	0.096 m	0.079 m
$O(\mu^2)$	0.0172	0.0157	0.0152	0.0279	0.0213	0.0289	0.0294
$O(\mu^4)$	0.0093	0.0104	0.0133	0.0153	0.0167	0.0130	0.0123

was very strong. Four measurement points were vertically distributed and numerical results were compared to measured values. The magnitude of horizontal velocity decreased with increasing submergence, as expected and showed a sharp increase on the wave front and more gentle decrease on the back side. Higher $O(\mu^4)$ results showed good agreement with measured values at all depths for both magnitude and phase. Small differences were noticeable near the times of maximum velocity, where details of the plunging jet would likely have been important and are not modeled in the present system. In contrast, the $O(\mu^2)$ system tended to overpredict velocities at both the crest and trough although overall agreement was still reasonable. A likely reason for this is that the quadratic velocity profile was unable to resolve the complexity of velocities in the breaking region.

Fig. 6 shows the variation of time-averaged horizontal velocity (undertow) with depth at all measurement locations for the plunging breaker. Negative undertow velocities near the bottom region can be seen for both sites while the mean surface velocity

is positive. The $O(\mu^4)$ system shows reasonable agreement, demonstrating that surf zone undertow can be modeled with this relatively simple breaking model, and giving good confidence moving forward for more complex three dimensional topographies. However, there are some differences for near-bed velocities in deeper depths, where a small secondary recurvature is observed in computations, but not in the data. This is likely a function of the q^4 vertical variation in velocity profiles, which is less complex than shown by the actual data. When decreasing order of approximation to $O(\mu^2)$, agreement with data declines. Again, this is likely a function of the limited z^2 velocity profile for the $O(\mu^2)$ model. Table 1 shows depth-averaged, dimensionless undertow error for both the $O(\mu^2)$ and $O(\mu^4)$ systems, demonstrating the significant increase in accuracy for the higher order system. When combined with the surface elevation and orbital velocity results, it appears that a higher order model will provide significant improvements to interior velocities, but is not as important in improving surface elevation results in the surf zone.
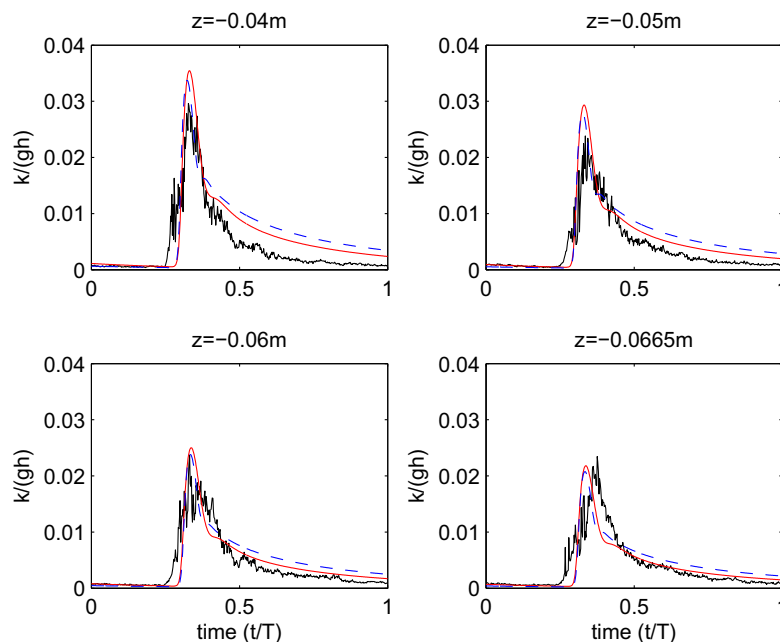

Fig. 7. Time-varying turbulent kinetic energy for plunging breaker at different points in the water column. $h/h_b = 0.584$, $h = 0.079m$. (—) $O(\mu^4)$ computed; (- -) $O(\mu^2)$ computed; (–) measured.
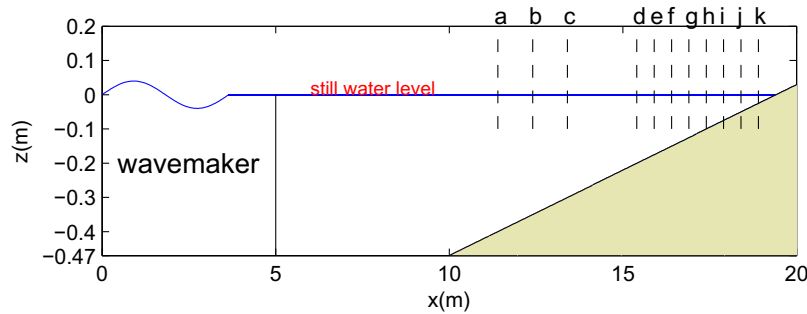
Fig. 8. Definition sketch for Mase and Kirby irregular wave tests. Depths for (a–k) are [0.4 0.35 0.3 0.2 0.175 0.15, 0.125, 0.075, 0.025] m.

Because the breaking system developed and implemented here provides direct estimates of the turbulent kinetic energy, k, it becomes possible to compare with experimental values at different points in the water column as shown in Fig. 7. These results show predictions that match well the general behavior of the experimental data, with both $O(\mu^2)$ and $O(\mu^4)$ systems giving similar results. However, there appear non-negligible over-predictions of k at the times of maximum breaking, and overall agreement is not as good as with surface elevations or interior velocities. This increased error is to be expected to some degree, since higher order quantities like turbulent kinetic energy and shear stress are more difficult to model than interior velocities or surface elevations (Pope, 2003). Given the relatively simple mixing length model implemented here, agreement seems

reasonable but it remains likely that a more complete turbulence model would be able to provide non-negligible improvements in higher order turbulent quantities. (See Fig. 7)

4.2. Irregular wave breaking

For a test of irregular waves the experiments of Mase and Kirby (1992) were modeled. The irregular waves were generated in 47 cm-depth water transitioning to a 1:20 planar slope to the shoreline as described in Fig. 8. Fig. 9 shows a truncated time series of computed and measured surface elevations at 6 gauges. The computed result almost overtops the data for the 5 deepest gauges. However, as waves propagate near the shore, the computed elevation goes off a bit but the agreement is still good, and
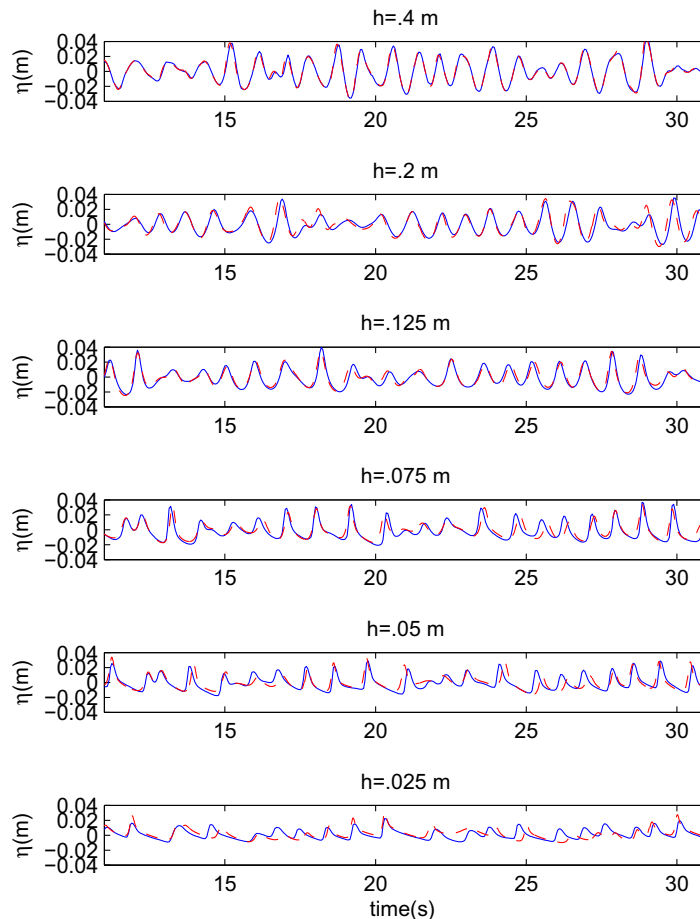

Fig. 9. Time series of surface elevation at different gauge locations. (- -) computed; (–) measured.
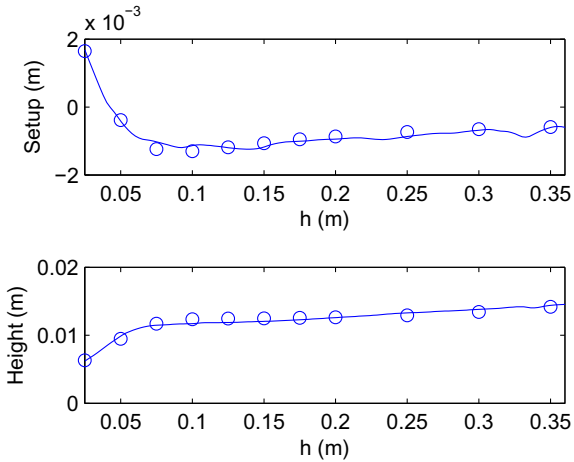
Fig. 10. Setup and wave height for Mase–Kirby irregular wave tests. (o) measured; (-) computed).
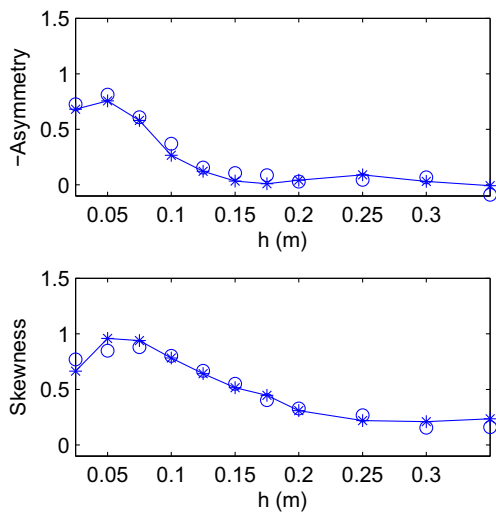

Fig. 11. Asymmetry and skewness for Mase–Kirby irregular wave tests. (o) measured; (-*-) computed.

Fig. 10 shows a good match for wave setup and wave height. Other statistical parameters can tell how well the model performs non-linearly. Wave asymmetry is a measure of left–right differences in a wave. Skewness is a measure of crest-trough shape. They are both computed from time series of surface elevation at chosen locations (Kennedy et al., 2000a). The computed results are compared with the data in Fig. 11. The trend is caught well from moderate depth through breaking to the shore. The wave becomes more asymmetric as propagating to the shore. The skewness increases as the wave shoals and breaks, and then decreases near the shoreline.

4.3. Solitary wave runup

As a check of the moving boundary algorithm, a runup test for a breaking solitary wave was simulated for a beach slope of $1/19.85$. The computed water surface runup for an initial solitary wave with wave height to still water depth ratio of $H/h = 0.3$ was compared to the experimental data by Synolakis (1987). Fig. 12 shows the water surface compared to the data during shoaling, breaking, runup and rundown. Panels 1, 2 and 3 show the wave becoming asymmetric followed by breaking in the surf zone. Panel 4 ($t = 25$) shows the breaking wave run up onto the beach and reaching near the highest point in Panel 5 ($t = 45$), while Panel 6 ($t = 50$) shows the rundown. Numerical results show good agreement with the data, providing a verification of the overall system for breaking and runup.

5. Discussion and conclusions

This paper is an extension and partial verification of the Boussinesq–Green–Naghdi rotational water wave model (Zhang et al., 2013). Due to the removal of the irrotationality assumption and the use of standard turbulence models, fewer ad hoc breaking assumptions have been made than many other eddy viscosity Boussinesq-type breaking models. Bottom friction and even surface wind shear stress can be added into the model by applying the boundary conditions when integrating the vertical force term in the momentum equation. Using simplifications to the well-known $k - l$ turbulence model, surf zone breaking phenomena such as wave height decay, setup, undertow velocities, and wave
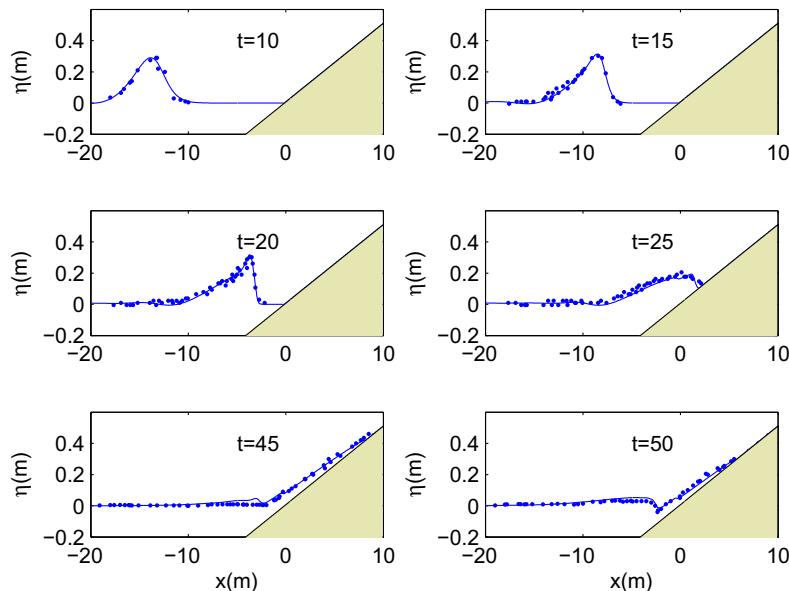

Fig. 12. Wave runup on a sloping beach. (·) measured; (–) computed.

runup are shown to be modeled well. One area of significant progress compared to some other Boussinesq surf zone models is the good agreement with the undertow velocity data which further validates the rotational feature of our model.

Both $O(\mu^2)$ and $O(\mu^4)$ systems were tested against each other and against experimental data. Results showed that the lower order systems performed very similarly to the higher order systems in computing wave heights and mean setup. In contrast, the more complex velocity profile found in the $O(\mu^4)$ system allowed for a significantly improved representation of both time-varying and time-averaged interior velocities. However there is still room for improvement. The mixing length profile used for breaking is highly approximate and might not represent the actual mixing length with high accuracy. This affects many quantities including the turbulent kinetic energy, k, which was not predicted as well as either surface elevations or interior velocities. A more complete turbulence model may be warranted for the future. The single-value surface assumption will additionally impose an upper limit on surf zone accuracy. However, the systems describe the overall breaking water surface, wave shape, rotational orbital velocities, and moving shoreline for wave runup reasonably well.

Although the tests herein provided a glimpse of the improved rotational capabilities of the model, further verification for two horizontal dimensions is necessary. This work is ongoing and will examine performance for breaking-driven flows where the lack of any irrotationality condition is expected to be important in modeling the interior velocities, and applications to geophysical and engineering problems.

Acknowledgments

Appendix A. Expressions for depth- integrated $O(\mu^2)$, $O(\mu^4)$ systems

The vertically integrated mass conservation equation is, to $O(\mu^2)$

$$\frac{\partial \eta}{\partial t} + \nabla \cdot \int_{-h}^{\eta} \mathbf{u}\,dz = \eta_{,t} + \nabla \cdot \left(\sum_{n=1}^{2} \mu^{\beta_n} \mathbf{u}_n (\eta+h) g_n|_{q=1} \right) = 0. \quad (A.1)$$

where g_n is defined in Appendix B.

Weighted momentum equation keeping all terms to $O(\mu^2)$ are

$$\mathbf{u}_{0,t}(\eta+h)g_m|_{q=1} + \mathbf{u}_0 \cdot \nabla \mathbf{u}_0 (\eta+h) g_m|_{q=1} + g\nabla\eta(\eta+h)g_m|_{q=1}$$
$$+ \mu^2 \sum_{n=1}^{2} \left(\mathbf{u}_{n,t}(\eta+h)\phi_{mn} - \mathbf{u}_n \eta_{,t}\varepsilon_{mn} \right)|_{q=1} - \mu^2 \left[\frac{1}{2} \nabla(\nabla \cdot \mathbf{u}_{0,t})(\eta+h)^3 \right.$$
$$\times (g_m - v_m) + (\nabla \cdot \mathbf{u}_{0,t})(\eta+h)^2 \nabla(\eta+h)g_m + \nabla(\mathbf{u}_{0,t} \cdot \nabla h)(\eta+h)^2$$
$$\times (g_m - S_m) + \mathbf{u}_{0,t} \cdot \nabla h \nabla \eta (\eta+h)g_m - (\nabla \cdot \mathbf{u}_{0,t})(\eta+h)^2 \nabla h S_m]|_{q=1}$$
$$+ \mu^2 \sum_{n=1}^{2} [(\mathbf{u}_n \cdot \nabla \mathbf{u}_0 + \mathbf{u}_0 \cdot \nabla \mathbf{u}_n)(\eta+h)\phi_{mn} - \mathbf{u}_n \nabla \cdot (\mathbf{u}_0(\eta+h))\varepsilon_{mn}]|_{q=1}$$
$$+ \mu^2 (\eta+h)^2 [(\nabla \cdot \mathbf{u}_0)^2 - \mathbf{u}_0 \cdot \nabla(\nabla \cdot \mathbf{u}_0)](\nabla\eta g_m + \nabla h(g_m - S_m))|_{q=1}$$
$$+ \frac{\mu^2}{2}(\eta+h)^3 \nabla[(\nabla \cdot \mathbf{u}_0)^2 - \mathbf{u}_0 \cdot \nabla(\nabla \cdot \mathbf{u}_0)](g_m - v_m)|_{q=1} - \mu^2(\eta+h)$$
$$\times \nabla\eta \mathbf{u}_0 \cdot \nabla(\mathbf{u}_0 \cdot \nabla h)g_m|_{q=1} - \mu^2(\eta+h)^2 \nabla(\mathbf{u}_0 \cdot \nabla(\mathbf{u}_0 \cdot \nabla h))(g_m - S_m)|_{q=1}$$
$$- \int_{-h}^{\eta} f_m \frac{\partial \tau_{xz}}{\partial z}\,dz - \int_{-h}^{\eta} \mu^2 f_m \nabla \cdot \tau_{xx}\,dz = 0, \quad m = 0,1,2. \quad (A.2)$$

The vertically integrated mass conservation equation is, to $O(\mu^4)$

$$\frac{\partial \eta}{\partial t} + \nabla \cdot \int_{-h}^{\eta} \mathbf{u}\,dz = \eta_{,t} + \nabla \cdot \left(\sum_{n=1}^{4} \mu^{\beta_n} \mathbf{u}_n (\eta+h) g_n|_{q=1} \right) = 0. \quad (A.3)$$

The integrated conservation of momentum equations for $O(\mu^4)$ level are

$$(\mathbf{u}_{0,t}(\eta+h) + \mathbf{u}_0 \cdot \nabla \mathbf{u}_0(\eta+h) + g\nabla\eta(\eta+h))g_m|_{q=1} + \mu^2(\ldots)$$
$$+ \sum_{n=3}^{N} \mu^{\beta_n} h\mathbf{u}_{n,t}\phi_{mn}|_{q=1} - \sum_{n=1}^{N-2} \mu^{\beta_n}[h\nabla(h^2\nabla \cdot \mathbf{u}_{n,t})(G_n|_{q=1}g_m|_{q=1}$$
$$- \Gamma_{mn}|_{q=1}) - h^2\nabla \cdot \mathbf{u}_{n,t}\nabla h(\gamma_{mn}|_{q=1} - \theta_{mn}|_{q=1}) + h\nabla(h(\mathbf{u}_{n,t} \cdot \nabla h))$$
$$\times ((g_n - R_n)|_{q=1}g_m|_{q=1} - \gamma_{mn}|_{q=1} + \Theta_{mn}|_{q=1}) + h(\mathbf{u}_{n,t} \cdot \nabla h)\nabla h$$
$$\times (\rho_{mn}|_{q=1} - F_{mn}|_{q=1} - \phi_{mn}|_{q=1} + \Psi_{mn}|_{q=1})] - \int_{-h}^{\eta} f_m \frac{\partial \tau_{xz}}{\partial z}\,dz$$
$$- \int_{-h}^{\eta} \mu^2 f_m \nabla \cdot \tau_{xx}\,dz = 0, \quad m = 0,1,2,3,4. \quad (A.4)$$

For both $O(\mu^2)$ and $O(\mu^4)$ systems, depth-integrated stress terms are given by (2.10) and (2.11).

Appendix B. Integral functions

All indefinite integrals will be assumed to have integration constants defined to give values of 0 at $q = 0$. Thus, for example, $g_n|_0^{q=1} = g_n|_{q=1}$.

$$g_n = \int f_n\,dq \qquad r_n = \int f_n'q\,dq \qquad G_n = \int g_n\,dq \qquad \psi_{mnv} = \int f_m'f_n'f_v\,dq$$
$$R_n = \int r_n\,dq \qquad \phi_{mn} = \int f_m f_n\,dq \qquad \gamma_{mn} = \int f_m g_n\,dq \qquad \zeta_{mn} = \int f_m f_n'\,dq$$
$$\rho_{mn} = \int f_m r_n\,dq \qquad \Gamma_{mn} = \int f_m G_n\,dq \qquad \Theta_{mn} = \int f_m R_n\,dq \qquad E_{mn} = \int f_m' f_n'\,dq$$
$$\theta_{mn} = \int f_m g_n q\,dq \qquad v_m = \int q^2 f_m\,dq \qquad S_m = \int q f_m\,dq \qquad K_{mn} = \int f_m' f_n' q^2\,dq$$
$$\varepsilon_{mn} = \int f_m f_n' q\,dq \qquad \Psi_{mn} = \int f_m f_n q\,dq \qquad F_{mn} = \int f_m r_n q\,dq \qquad J_{mn} = \int f_m' f_n' q\,dq$$

References

Benque, J.P., Cunge, J.A., Hauguel, J.F., Holly, F.M.A., 1982. New method for tidal current circulation. J. Waterway Port Coastal Ocean Div.-ASCE 108, 396–417.

Bonneton, P., Barthelemy, E., Chazel, F., Cienfuegos, R., Lannes, D., Marche, F., Tissier, M., 2011. Recent advances in Serre–Green Naghdi modelling for wave transformation, breaking, and runup. Eur. J. Mech. B-Fluids 30, 589–597.

Boussinesq, J., 1877. Essai sur la théorie des eaux courantes. Mémoires présentés par divers savants à l'Académie des Sciences XXIII, 1–680.

Chen, Q., Kirby, J.T., Dalrymple, R.A., Kennedy, A.B., Chawla, A., 2000. Boussinesq modeling of wave transformation, breaking, and runup. II: 2D. J. Waterway Port Coastal Ocean Eng. 126, 48–56.

Cienfuegos, R., Barthelemy, E., Bonneton, P., 2010. Wave-breaking model for Boussinesq-type equations including roller effects in the mass conservation equation. J. Waterway Port Coastal Ocean Eng. 136, 10–26.

Ertekin, R.C., Webster, W.C., Wehausen, J.V., 1986. Waves caused by a moving disturbance in a shallow channel of finite width. J. Fluid Mech 169, 275–292.

Gallerano, F., Cannata, G., Villani, M., 2014. An integral contravariant formulation of the fully non-linear Boussinesq equations. Coastal Eng. 83, 119–136.

Gobbi, M.F., Kirby, J.T., 1999. Wave evolution over submerged sills: tests of a high-order Boussinesq model. Coastal Eng. 37, 57–96, and erratum, Coastal Eng. 40, 277.

Gobbi, M.F.G., Kirby, J.T., Wei, G., 2000. A fully nonlinear Boussinesq model for surface waves. II. Extension to $O(\mu^4)$. J. Fluid Mech. 405, 181–210.

Green, A.E., Naghdi, P.M., 1976. A derivation of equations for wave propagation in water of variable depth. J. Fluid Mech. 78, 237–246.

Higuera, P., Lara, J.L., Losada, I.J., 2013. Simulating coastal engineering processes with OpenFOAM. Coastal Eng. 71, 119–134.

Kennedy, A.B., Chen, Q., Kirby, J.T., Dalrymple, R.A., 2000a. Boussinesq modeling of wave transformation, breaking, and runup. I: 1D. J. Waterway Port Coastal Ocean Eng. 126, 39–47.

Kennedy, A.B., Dalrymple, R.A., Kirby, J.T., Chen, Q., 2000b. Determination of inverse depths using direct Boussinesq modeling. J. Waterway Port Coastal Ocean Eng. 126, 206–214.

Kennedy, A.B., Kirby, J.T., Chen, Q., Dalrymple, R.A., 2001. Boussinesq-type equations with improved nonlinear performance. Wave Motion 33, 225–243.

Kim, D.-H., Lynett, P.J., 2013. A sigma-coordinate transport model coupled with rotational Boussinesq-type equations. Environ. Fluid Mech. 13, 51–72.

Kim, J.W., Bai, K.J., Ertekin, R.C., Webster, W.C., 2003. A strongly-nonlinear model for water waves in water of variable depth – the irrotational Green–Naghdi model. J. Offshore Mech. Arctic Eng. 125, 25–32.

Klonaris, G.Th., Memos, C.D., Karambas, Th.V., 2013. A Boussinesq-type model including wave-breaking terms in both continuity and momentum equations. Ocean Modell. 57, 128–140.

Lynett, P.J., Liu, P.L.F., 2002. A two-dimensional, depth-integrated model for internal wave propagation over variable bathymetry. Wave Motion 36, 221–240.

Lynett, P.J., Wu, T.R., Liu, P.L.F., 2002. Modeling wave runup with depth-integrated equations. Coastal Eng. 46, 89–107.

Madsen, P.A., Schäffer, H.A., 1998. Higher order Boussinesq-type equations for surface gravity waves- derivation and analysis. Philos. Trans. R. Soc. A 356, 1–59.

Madsen, P.A., Srensen, O.R., 1992. A new form of the Boussinesq equations with improved linear dispersion characteristics. Part 2. A slowly varying bathymetry. Coastal Eng. 18, 183–204.

Madsen, P., Srensen, O., Schäffer, H., 1997. Surf zone dynamics simulated by a Boussinesq-type model: Part I. Model description and cross-shore motion of regular waves. Coastal Eng. 32, 255–288.

Ma, G., Shi, F.Y., Kirby, J.T., 2012. Schock-capturing non-hydrostatic model for fully dispersive surface wave processes. Ocean Modell. 43–44, 22–35.

Mase, H., Kirby, J.T., 1992. Hybrid frequency-domain KdV equation for random wave transformation. In: Proceedings of 23rd International Coastal Engineering Conference,. ASCE, New York, pp. 474–487.

Musumeci, R.E., Svendsen, I.A., Veeramony, J., 2005. The flow in the surf zone: a fully nonlinear Boussinesq-type of approach. Coastal Eng. 52, 565–598.

Nezu, I., Rodi, W., 1986. Open-channel flow measurements with a laser doppler anemometer. J. Hydraulic Eng. 112 (5), 335–355.

Nwogu, O., 1993. Alternative form of Boussinesq equations for nearshore wave propagation. J. Waterway Port Coastal Ocean Eng. 119, 618–638.

Nwogu, O., Demirbilek, Z., 2010. Infragravity wave motions and runup over shallow fringing reefs. J. Waterway, Port, Coastal and Ocean Eng. 136 (6), 295–305.

Peregrine, D.H., 1967. Long waves on a beach. J. Fluid Mech. 27, 815827.

Pope, S.B., 2003. Turbulent Flows. Cambridge University Press, Cambridge.

Richard, G.L., Gavrilyuk, S.L., 2012. A new model of roll waves: comparison with Brock's experiments. J. Fluid Mech. 698, 374–405.

Schäffer, H.A., Madsen, P.A., 1993. A Boussinesq model for waves breaking in shallow water. Coastal Eng. 20, 185–202.

Shields, J.J., Webster, W.C., 1988. On direct methods in water-wave theory. J. Fluid Mech. 197, 171–199.

Shi, F.Y., Kirby, J.T., Harris, J.C., Geiman, J.D., Grilli, S.T., 2012. A high-order adaptive time-stepping TVD solver for Boussinesq modeling of breaking waves and coastal inundation. Ocean Modell. 43–44, 36–51.

Srensen, O.R., Schäffer, H.A., Madsen, P.A., 1998. Surf zone dynamics simulated by a Boussinesq type model. III Wave-induced horizontal circulations. Coastal Eng. 33, 155–176.

Svendsen, I., 1984. Mass flux and undertow in a surf zone. Coastal Eng. 8, 347365.

Synolakis, C.E., 1987. The run-up of solitary waves. J. Fluid Mech. 185, 523–545.

Ting, F.C.K., Kirby, J.T., 1994. Observation of undertow and turbulence in a laboratory surf zone. Coastal Eng. 24, 5180.

Ting, F.C.K., Kirby, J.T., 1995. Dynamics of surf-zone turbulence in a strong plunging breaker. Coastal Eng. 24, 177204.

Ting, F.C.K., Kirby, J.T., 1996. Dynamics of surf-zone turbulence in a spilling breaker. Coastal Eng. 27, 131160.

Tissier, M., Bonneton, P., Marche, F., Chazel, F., Lannes, D., 2012. A new approach to handle wave breaking in fully non-linear Boussinesq models. Coastal Eng. 67, 54–66.

Veeramony, J., Svendsen, I.A., 2000. The flow in surf-zone waves. Coastal Eng. 39, 93–122.

Wei, G., Kirby, J.T., Grilli, S.T., Subramanya, R., 1995. A fully nonlinear Boussinesq model for surface waves. I. Highly nonlinear, unsteady waves. J. Fluid Mech. 294, 71–92.

Zelt, J.A., 1991. The runup of nonbreaking and breaking solitary waves. Coastal Eng. 15, 205246.

Zhang, Y., Kennedy, A.B., Panda, N., Dawson, C., Westerink, J.J., 2013. Boussinesq–Green–Naghdi rotational water wave theory. Coastal Eng. 73, 13–27.

Zhang, Y., Kennedy, A.B., Panda, N., Dawson, C., Westerink, J.J., 2014a. Generating-absorbing sponge layers for phase-resolving wave models. Coastal Eng. 84, 1–9.

Zhao, B.B., Duan, W.Y., Ertekin, R.C., 2014b. Application of higher-level GN theory to some wave transformation problems. Coastal Eng. 83, 177–189.